Energy & Environmental Science

PAPER

View Article Online
View Journal | View Issue

Cite this: *Energy Environ. Sci.*, 2014, **7**, 1454

A diketopyrrolopyrrole-containing hole transporting conjugated polymer for use in efficient stable organic–inorganic hybrid solar cells based on a perovskite†

Young Soo Kwon,‡[a] Jongchul Lim,‡[a] Hui-Jun Yun,[b] Yun-Hi Kim*[b] and Taiho Park*[a]

Received 26th December 2013
Accepted 27th January 2014

DOI: 10.1039/c3ee44174a

www.rsc.org/ees

Poly[2,5-bis(2-decyldodecyl)pyrrolo[3,4-*c*]pyrrole-1,4(2*H*,5*H*)-dione-(*E*)-1,2-di(2,2′-bithiophen-5-yl) ethene] (PDPPDBTE) was successfully incorporated as a p-type hole transporting material in solid-state organic–inorganic hybrid solar cells. The excellent optical and electrical properties of organo-lead halide perovskite ($CH_3NH_3PbI_3$) nanocrystals used as light harvesters yielded a 9.2% power conversion efficiency (PCE) for the best-performing cell that exceeded the value (7.6%) obtained from the best hole conductor yet reported (2,2′,7,7′-tetrakis(*N*,*N*-di-*p*-methoxyphenyl-amine)9,9′-spirobifluorene, spiro-MeOTAD). The high PCE was attributed to the optimal oxidation potential (5.4 eV) and excellent charge carrier mobility of the polymer. The hydrophobicity of the polymer prevented water permeation into the porous perovskite heterojunction, and long-term aging tests over 1000 hours confirmed the enhanced stability of the PDPPDBTE-based cells.

Broader context

Solid-state organic–inorganic hybrid solar cells have been extensively investigated as an alternative promising energy conversion devices to the conventional silicon-based photovoltaics. With the successful demonstration of the solar cells which utilize lead halide perovskite nanocrystals as excellent light harvesters the overall efficiencies rapidly increased during the last year, yielding over 15% of remarkable performance. Further enhancement of the efficiency could be realized by developing new hole transporting materials with high electrical properties and proper oxidation potential with respect to the energy level of perovskite. To this end, the conjugated polymers are thought to be an alternative to small molecular hole conductors since they have unique charge transport properties with tunable oxidation potential. In this work, we report an efficient stable hybrid solar cells incorporating diketopyrrolopyrrole-containing polymers (PDPPDBTE). With an appropriate oxidation potential of 5.4 eV *vs.* the vacuum level, the PDPPDBTE conjugated polymer is expected to function efficiently as a hole transporting material. Furthermore, the excellent long-term stability of polymer-based solar cells also guarantee their potential applications.

Introduction

Solid-state organic–inorganic hybrid solar cells have been studied extensively since their first demonstration in 1998 by Bach *et al.*[1] Recent developments in light absorber materials based on lead halide perovskite nanocrystals[2–10] have yielded power conversion efficiencies (PCEs) exceeding 15% in hybrid solar cells.[5,6] Efficient light-absorbing sensitizers and inorganic semiconducting oxides must be paired with an efficient organic hole transporting material (HTM) to establish appropriate regenerative cycles from the holes in the oxidized sensitizers anchored on the oxide surfaces. A molecular HTM, 2,2′,7,7′-tetrakis(*N*,*N*-di-*p*-methoxyphenylamine)-9,9′-spirobifluorene (spiro-MeOTAD), has exhibited the best performance to date due to its high glass transition temperature, high solubility, appropriate oxidation potential, absorption spectrum, and amorphous structure.[11] Despite offering the best performance yet achieved in an HTM, spiro-MeOTAD suffers from a low hole mobility ($\sim 10^{-4}$ cm^2 V^{-1} s^{-1}) and a low conductivity ($\sim 10^{-5}$ S cm^{-2}) in its pristine form.[12,13] Additional additives or p-type dopants are required for applications. Lithium salts, such as lithium bis(trifluoromethylsulfonyl)-imide (Li-TFSI), are commonly mixed with spiro-MeOTAD to adjust the material's properties. Li-TFSI tends to introduce p-doping into a broad range of polymers and small molecule organic semiconductors, dramatically increasing the conductivity and hole mobility.[13] Burschka *et al.* reported that the presence of an additional p-type cobalt complex dopant greatly enhanced the performance of solar cells, mainly by generating a high fill factor.[12] A low series resistance for charge transport is important for HTMs.

[a]*Department of Chemical Engineering, Pohang University of Science and Technology, Pohang, Gyungbuk, Korea. E-mail: taihopark@postech.ac.kr*

[b]*Department of Chemistry, Gyungsang National University and Research Institute of Nature Science, Jinju, Gyungnam, Korea. E-mail: ykim@gnu.ac.kr*

† Electronic supplementary information (ESI) available: Fig. S1–S5. See DOI: 10.1039/c3ee44174a

‡ These authors contributed equally to this work.

Alternative HTM materials with excellent electrical properties may be used in place of spiro-MeOTAD; however, few such materials are available. Donor–π–Acceptor conjugated polymers are candidate alternatives and have been widely used as active conductive materials in a variety of soft electronics owing to their unique and tunable optical and electrical properties, with a low production cost and a versatile wet processing procedure. Organic field effect transistors (OFETs), organic light-emitting diodes (OLEDs), and organic bulk heterojunction (BHJ) solar cells have been successfully prepared using numerous conjugated polymers, with remarkable performances.[14–18] In the field of hybrid solar cells, however, only a few conductive polymers have provided reliable performances, despite displaying excellent electrical properties in the context of other organic electronics.[19–21] During the initial stages of hybrid solar cell research, major limitations associated with the polymer properties, such as a significant spectral overlap with the light absorbing sensitizer and poor pore penetration into the mesoporous oxide films, hampered their efficient operation.[22] In the latter case, unfilled regions acted as defect sites for charge regeneration, and an extremely thin absorber (ETA) layer less than 1 μm thick was required to realize good pore penetration.

Recent advances in the use of perovskite-sensitized or "meso superstructured" solar cells have opened up new possibilities for using a variety of hole transporting polymers (HTPs) because ETA layers could be used to ensure efficient pore penetration without significant loss of the light harvesting ability. Heo *et al.* reported a ~12% PCE in an organic–inorganic hybrid solar cell using a poly(triarylamine) (PTAA) HTP with an average performance of ~9.5%.[7] They suggested that the unique ambipolar properties of perovskites efficiently transferred charges at the TiO_2/perovskite (p-type) and perovskite/HTP (n-type) heterojunctions within the pillared mesostructure; however, no D–π–A conjugated polymer has yet been reported to offer a performance better than that of spiro-MeOTAD. Diketopyrrolopyrrole (DPP)-containing conjugated conducting polymers have been incorporated with a perovskite, yielding a 5.55% PCE whereas a spiro-MeOTAD cell exhibited 6.8%.[9] A more detailed characterization of DPP-based polymers could expand the practical utility of this system in hybrid solar cells.

We recently reported the development of DPP-based highly π-extended polymers, namely, poly[2,5-bis(2-decyldodecyl)-pyrrolo[3,4-*c*]pyrrole-1,4(2*H*,5*H*)-dione-(*E*)-1,2-di(2,2′-bithio phen-5-yl)-ethene] (PDPPDBTE), which provided high-performance field effect transistors that exhibited a $\mu_{FET} = 0.32\ cm^2\ V^{-1}\ s^{-1}$.[23] The DPP moiety exhibited excellent hole mobilities in OFETs and successfully functioned in organic photovoltaics (OPVs).[24,25,36] With an appropriate oxidation potential of 5.4 eV *vs.* the vacuum level, the PDPPDBTE conjugated polymer is expected to function efficiently as an HTP when incorporated into perovskite-based hybrid solar cells.

Herein, we report the preparation of efficient solid-state hybrid solar cells using PDPPDBTE as a HTP. A PCE of 9.2% was achieved, along with excellent long-term stability over 1000 h. To our knowledge, this is the first successful demonstration of a conjugated polymer-based solar cell with a PCE exceeding the maximum value obtained from a spiro-MeOTAD-based solar cell (7.6%). Considering that the averaged PCE of a perovskite cell prepared using spiro-MeOTAD lies between 7.5 and 8.5%, further performance enhancements are expected of PDPPDBTE-based cells with careful optimization of the device architecture. Fig. 1a and b show the chemical structures and relative energy levels of the HTMs used in this study and P3HT, which was tested to allow a comparison with conventional conjugated HTPs.

Experimental section

Synthesis of a $CH_3NH_3PbI_3$ perovskite

The $CH_3NH_3PbI_3$ perovskite was prepared according to the reported procedure.[3] CH_3NH_3I, to be used as a light harvester, was synthesized by reacting 27.86 ml methylamine (40% in methanol, Junsei Chemical Co.) and 30 ml hydroiodic acid (57 wt% in water, Aldrich) in a 250 ml round-bottomed flask at 0 °C for 2 h with stirring. The precipitate was recovered by evaporation at 50 °C for 1 h followed by washing three times with diethyl ether and filtered off using a Buchner funnel. The product was then dissolved in ethanol, recrystallized from diethylether, and dried at 60 °C in a vacuum oven for 24 h The synthesized CH_3NH_3I powder was mixed with PbI_2 (Aldrich) at a 1 : 1 molar ratio in γ-butyrolactone at 60 °C for 12 h, followed by filtering twice using a PVDF syringe filter (Whatman, 0.45 μm). The concentration of $CH_3NH_3PbI_3$ was 40 wt%.

Solar cell fabrication

The fabrication of a solid-state hybrid solar cell is reported elsewhere.[7] A 80 nm thick layer of dense blocking TiO_2 (bl-TiO_2) was coated onto a F-doped SnO_2 (FTO, Pilkington, TEC8) substrate by spray pyrolysis deposition of titanium diisopropoxide bis(acetylacetonate) (Aldrich) solution which is diluted with ethanol (1 : 10 v/v) at 250 °C to prevent direct contact between the FTO and hole conducting layer. Mesoporous TiO_2 (mp-TiO_2) films with 600 nm thickness was then deposited by spin coating of a diluted TiO_2 paste (Dyesol 18NR-T, 1 : 2.5 w/w diluted with ethanol) at 2500 rpm for 40 s. The films were calcined at 500 °C for 1 h to remove the organic part. The films were then immersed into 20 mM of $TiCl_4$ aqueous solution at 60 °C for 1 h and heat-treated at 500 °C for 30 min to improve interfacial contact with the nanocrystalline TiO_2.

The $CH_3NH_3PbI_3$/γ-butyrolactone solution was then coated onto the mp-TiO_2/bl-TiO_2/FTO substrate by spin-coating at 2000 rpm, 60 s and 3000 rpm, 60 s. As spun films were then dried on a hot plate at 100 °C for 5 min. The P3HT was purchased from Rieke and used without further purification. The HTMs were spin-coated onto the $CH_3NH_3PbI_3$/mp-TiO_2/bl-TiO_2/FTO substrate at 3000 rpm for 30 s using HTMs/1,2-dichlorobenzene (15 mg/1 ml) with 20.4 μl Li-bis(trifluoromethanesulfonyl) imide (Li-TFSI)/acetonitrile (28.3 mg/1 ml) and 10.2 μl TBP as additives. A spiro-MeOTAD (Merck KGaA)/chlorobenzene (180 mg/1 ml) solution was used with added 37.5 μl Li-bis(trifluoromethanesulfonyl) imide (Li-TFSI)/acetonitrile (170 mg/1 ml) and 17.5 μl TBP. Finally, a gold counter electrode was

deposited by thermal evaporation. The active area was fixed at 0.09 cm^2.

Device characterization

The IPCE spectra were recorded as functions of wavelength under a constant white light bias of approximately 5 mW cm^{-2} supplied by an array of white light emitting diodes using a power source with a monochromator (Zahner GmbH) and a multimeter and chopped at approximately 5 Hz. The current density–voltage (*J–V*) curves were measured with a solar simulator (Newport, Oriel Class A, 91195A) with a source meter (Keithley 2420) at a 100 mA cm^{-2} illumination (AM 1.5G) and a calibrated Si-reference cell equipped with an IR cutoff filter (KG-3, Schott) certificated by NREL. The *J–V* curves of all devices were measured by masking the active area with a metal mask of area 0.09 cm^2. The long-term stability of a solar cell was tested over 1000 h, while the device was stored under atmospheric conditions in the dark where the humidity was kept approximately at 20% without encapsulation.

Transient mobility spectroscopy

Devices for measuring the conductivity of the HTMs were prepared according to a published procedure.[13] The preparation (on glass substrates) was identical to that used for the solid-state hybrid solar cell, the differences being that no compact layer of TiO_2 was deposited, C106 NaRu(4,4-bis(5-(hexylthio)-thiophen-2-yl)-2,2-bipyridine) (4-carboxylic acid-4-carboxylate-2,2-bipyridine) $(NCS)_2$ dye was sensitized onto the TiO_2 electrode, and the electrode pattern was designed for two point probe measurements with a channel length (direction of current flow) of 300 μm, a channel width of 6.53 cm, and a film thickness of 1 μm. The gold electrodes were 200 nm thick to ensure that light was only passed between the electrodes. Transient absorption and photoconductivity measurements were performed simultaneously on the conductivity devices. An Nd:YAG laser was used at a 550 nm pump wavelength and laser intensity 35 mJ, which was adapted *via* optical filters to 50 μJ cm^{-2} for the current extraction measurements, at a 10 ns pulse length and 10 Hz repetition rate.

Results and discussion

A typical organic–inorganic hybrid solar cell structure is shown in Fig. 1c, with the configuration of mesoporous (mp) TiO_2/$CH_3NH_3PbI_3$/HTM/Au. A 600 nm thick mp-TiO_2 layer was deposited by spin-coating a diluted TiO_2 paste (Fig. 1d) onto a substrate. The thickness was selected based on the results obtained from several previous studies of the effect of the layer thickness on device performance.[4,5] Unlike the previously reported solid-state hybrid solar cells that used ruthenium or an organic dye, perovskite nanocrystals with unique optical properties enabled the use of an ETA layer with nearly a 100% light harvesting efficiency at the peak wavelength, excluding losses associated with absorption by the FTO and the glass substrate.[26] The $CH_3NH_3PbI_3$ layer was then applied to the porous network using a simple spin-coating process. Complete pore infiltration was ensured under these conditions. Recently, Heo *et al.* reported the preparation of efficient hybrid solar cells that yielded a 12.0% PCE. They suggested that the $CH_3NH_3PbI_3$ perovskites only partially infiltrated the porous TiO_2 film to create a capping layer on top of the TiO_2 layer that formed a "pillared structure" composed of perovskite/HTMs.[7]

The perovskite deposition process was optimized by varying the spin-coating speed. The trends in the resulting photovoltaic performances are summarized in Fig. S1.† Despite the absence of detailed studies of the effects of the perovskite capping layer on device performance, our results suggested that the predominant uniform penetration of the perovskite into the mesoporous film was important for the device performance as well as to ensure reproducibility in commercial applications. A recent report described the importance of minimizing morphological variations by sequentially depositing perovskite precursors.[5]

Cross-sectional scanning electron microscopy (SEM) images and energy dispersive X-ray spectral (EDS) analysis verified the

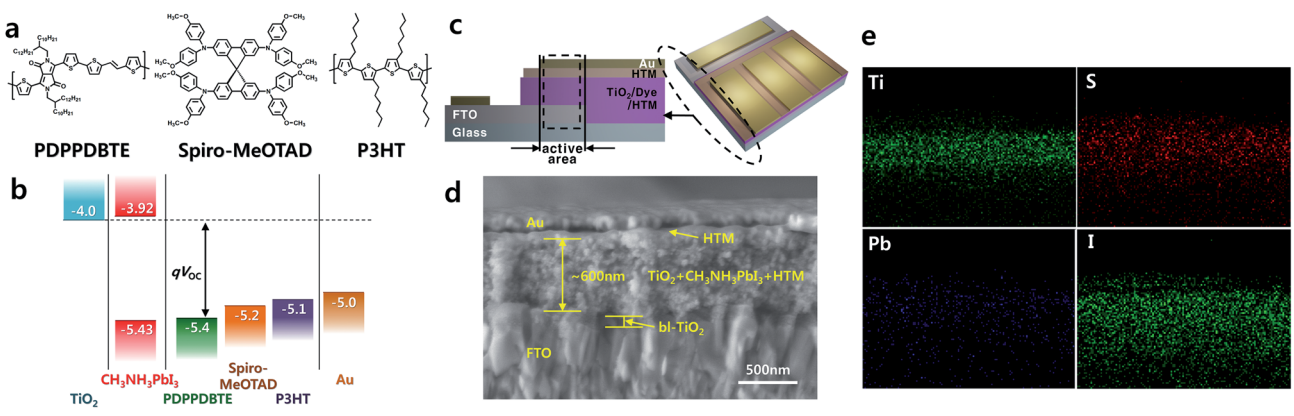

Fig. 1 (a) Chemical structures of the hole transport materials PDPPDBTE, spiro-MeOTAD, and P3HT used in this study. (b) The relative energy levels of each component in a hybrid solar cell. (c) Schematic diagram of the device structure, and (d) SEM cross-sectional images of the solid-state hybrid solar cell prepared using PDPPDBTE as an HTP. (e) Cross-sectional energy dispersive X-ray spectral (EDS) mapping of the Ti, S, Pb, and I elements in the PDPPDBTE-based solid-state hybrid solar cell.

formation of a uniform distribution of the perovskites throughout the mesoporous oxide films (Fig. 1e, Pb and I elemental mapping). Finally, the devices were completed by depositing the HTMs (spiro-MeOTAD, P3HT, or PDPPDBTE) and gold counter electrodes. The concentrations of additives, including lithium bis(trifluoromethyl sulfonyl) imide (Li-TFSI) and *tert*-butylpyridine (tBP) were optimized in the HTPs (Fig. S2†).

A highly concentrated spiro-MeOTAD solution (180 mg ml^{-1} in chlorobenzene) produced an ~150 nm thick overlayer on top of the photoactive layer (data not shown), whereas a solution having a low concentration of the HTP (15 mg ml^{-1} in 1,2-dichlorobenzene) formed overlayers ~30 nm (Fig. 1d). Unlike the result obtained from hybrid solar cells prepared using other HTPs with a pillared structure,[7] the PDPPDBTE appeared to efficiently infiltrate the photoactive films, as revealed by EDS analysis and sulfur atom mapping, which revealed the distribution of the PDPPDBTE backbone (Fig. 1e, S elemental mapping). Secondary ion mass spectroscopy (SIMS) analysis and depth profiling of a hybrid solar cell prepared with PDPPDBTE confirmed this result (Fig. S3†).

The absorbance spectra of the perovskite-coated TiO_2 films are shown in Fig. 2a. The perovskite nanocrystals strongly absorbed light over the whole visible range, indicating efficient light absorption. Spiro-MeOTAD absorbed light at wavelengths shorter than 400 nm, which did not overlap with the absorption bands of perovskites (data not shown).

The HTP-coated photoactive films showed an additional peak absorbance at wavelengths of ~520 nm for P3HT and ~750 nm for PDPPDBTE. The HTP-coated TiO_2 films prepared without perovskites displayed the appropriate characteristic absorption peak. The additional absorption peak observed in the perovskite-containing devices was attributed to the polymer. The spectral overlap often reduces the efficiency of light harvesting by the perovskite and results in a loss of photocurrent in a solar cell. The excellent absorption profile of the perovskite did not allow such losses by the polymer, as demonstrated by the IPCE spectra (Fig. 2b). No IPCE peak over 800 nm wavelength for PDPPDBTE-based solar cells despite light absorption confirmed that the role of PDPPDBTE is limited to a charge transporting layer. The peak intensities of the IPCE spectra obtained from the 3 devices reached 70%, and *ca.* 20% of the incident light was scattered by the conducting FTO glass,[26] indicating that the absorbed light was efficiently transformed to a photocurrent in the perovskite-sensitized solar cells. The similar spectral shapes obtained from the 3 types of devices corroborated the conclusion that absorption by the polymer was negligible.

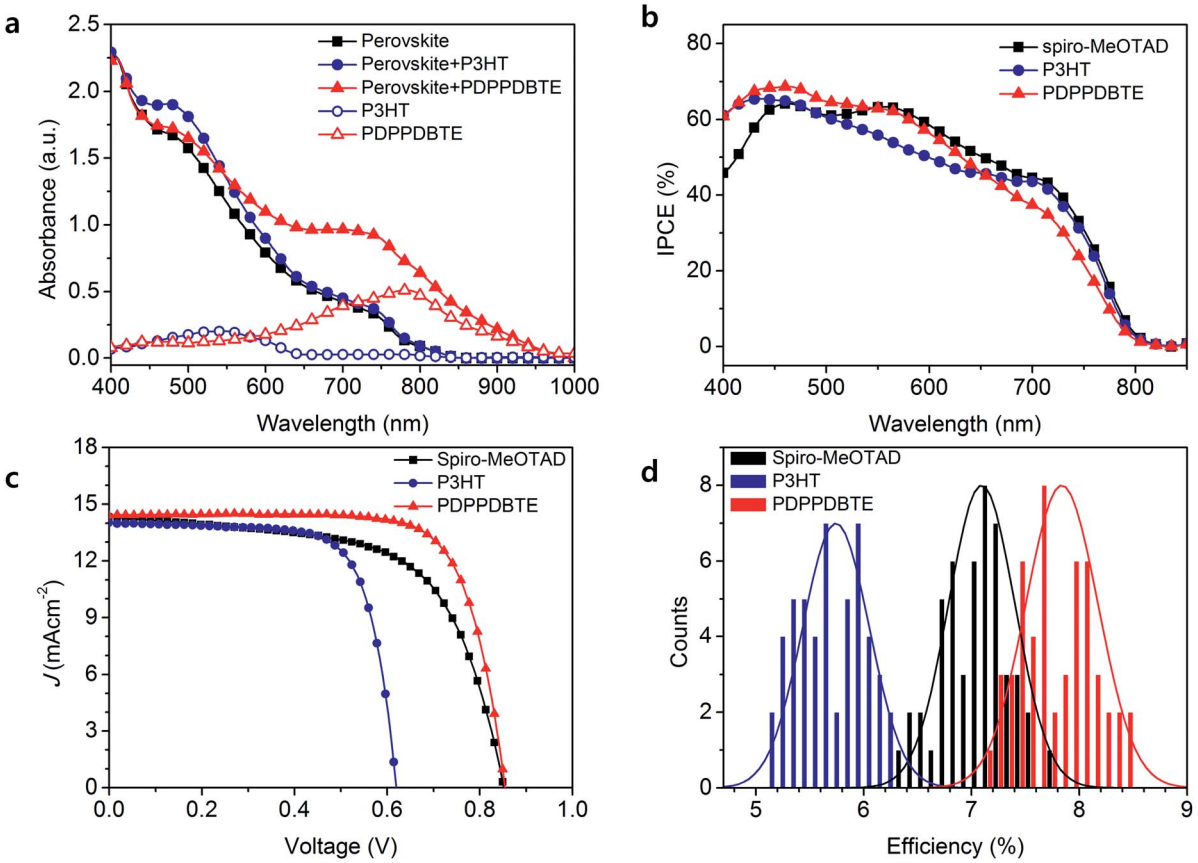

Fig. 2 (a) Absorbance spectra of FTO/bl-TiO_2/mp-TiO_2/$CH_3NH_3PbI_3$/HTM. (HTM-only coated films are indicated by the empty shapes.) (b) IPCE spectra of the solar cells prepared with different HTMs (c) *J*–*V* curves of the hybrid solar cells made from spiro-MeOTAD (black squares), P3HT (red circles), and PDPPDBTE (blue triangles) HTMs. (d) Histogram of the solar cell efficiencies obtained from 50 samples of the spiro-MeOTAD-, P3HT-, and PDPPDBTE-based hybrid solar cells. (Gaussian distributions were fit to obtain the average and standard deviations.)

We measured the current density–voltage (J–V) characteristics of the solar cells prepared from different HTMs under simulated air mass 1.5 global (AM 1.5 G) solar irradiation. Fig. 2c shows the J–V curves obtained from the best-performing solar cells among the 50 devices prepared using each HTM. The photovoltaic parameters are summarized in Table 1. The device prepared with spiro-MeOTAD exhibited a $J_{SC} = 14.3$ mA cm^{-2}, a $V_{OC} = 849.2$ mV, a FF = 62.5%, corresponding to a PCE = 7.6%. The device prepared with PDPPDBTE displayed a $J_{SC} = 14.4$ mA cm^{-2}, a $V_{OC} = 855.3$ mV, a FF = 74.9%, yielding a PCE = 9.2%. The device prepared with P3HT yielded a $J_{SC} = 14.0$ mA cm^{-2}, a $V_{OC} = 620.1$ mV, a FF = 72.2%, and a PCE = 6.3%, the lowest performances obtained from the devices prepared with other HTMs. Unlike solar cells prepared using spiro-MeOTAD, the best efficiency in a PDPPDBTE-based solar cell was achieved after storage for 24 hours under the ambient atmosphere without encapsulation. The other HTM-based solar cells displayed their best efficiencies immediately after fabrication. These observations indicated that the PDPPDBTE-based solar cells were stable, as discussed further below.

The similar J_{SC} values for the 3 devices agreed well with the results obtained from IPCE measurements. Whereas the J_{SC} values of the three types of devices were similar, the V_{OC} and fill factors differed significantly. The V_{OC} trends for the HTP-containing solar cells agreed well with the HOMO levels of the HTPs, which were 230 mV higher for the PDPPDBTE cells than that for the P3HT cells since the V_{OC} is theoretically estimated from the energy difference between the quasi-Fermi level of TiO_2 and the HOMO level of HTMs. Mixing the spiro-MeOTAD with higher additive concentrations to form the HTMs increased the V_{OC} value beyond what was expected based on the HOMO level under optimized conditions. The tBP additive is known to increase the density of state in TiO_2 and shift the conduction band of TiO_2 toward the vacuum level, increasing the V_{OC}.[27] The fill factor of the spiro-MeOTAD was apparently lower than that of the other HTP-based solar cells, whereas the fill factors of the PDPPDBTE cells provided the highest values. The reproducibility of the fabrication process was examined by fabricating and characterizing 50 solar cells. The statistical distribution of efficiencies obtained from the freshly prepared cells is displayed in Fig. 2d. The resulting device performances followed a Gaussian distribution and yielded average performances of 7.10%, 5.74%, and 7.84% for the spiro-MeOTAD, P3HT, and PDPPDBTE-based solar cells, respectively. Narrow standard deviations of ~0.3% for the 3 types of devices indicated good reproducibility.

It is worth noting that the J_{SC} of the PDPPDBTE cell was comparable to that obtained from the spiro-MeOTAD cell, despite the very small energetic driving force needed to regenerate the oxidized perovskite (30 mV). This result was explained by assuming that the slow charge transfer rate was compensated for by fast charge transport in an HTP medium. Indeed, the trend in the fill factors of the 3 devices could be explained under the assumptions described by Burschka *et al.*, who demonstrated that the conductivity of an organic semiconductor is important for achieving a high device performance.[12] These researchers developed a new cobalt complex that greatly enhanced the solar cell performance mainly due to an increase in the fill factor. The relationship between the fill factor and the conductivity (or the charge carrier mobility) of the 3 HTMs was examined by performing transient mobility spectroscopy (TMS), introduced recently as a tool for measuring the charge carrier mobility as a function of the charge density in a mesostructured TiO_2/dye/HTM heterojunction.[13] Transient absorption spectroscopy (TAS), in combination with time resolved photo-conductivity measurements permitted extraction of the photoinduced electron or hole carrier density and the conductivity to yield the estimated mobility over a broad range of charge densities. The device geometry employed for the TMS measurements is summarized in the Experimental section.

Here, we sensitized a ruthenium dye, C106,[28,29] rather than the perovskites due to difficulties associated with distinguishing the changes in the absorption spectra of the oxidized HTMs and the perovskite due to a spectral overlap. A C106-sensitized TiO_2 film infiltrated with 3 HTMs was used to characterize the characteristic absorption spectra of the oxidized forms of the HTMs in the visible to near IR region. These results revealed the direct relationship between the absorption changes and the hole density in the HTMs. The extinction coefficients of the 3 HTMs were initially measured in an effort to relate the changes in the absorption spectra of the oxidized HTMs to the photoinduced charge density, yielding 33 500 M^{-1} cm^{-1} for the spiro-MeOTAD at 505 nm, 53 500 M^{-1} cm^{-1} for P3HT at 700 nm, and 20 500 M^{-1} cm^{-1} for PDPPDBTE at 930 nm, respectively. These results were consistent with the results obtained from previous studies.[13]

The effective mobilities of the 3 HTMs prepared without additives are plotted in Fig. 3a. Undoped HTMs were used to measure the mobilities; the charge density prior to laser perturbation was non-negligible if the material had been chemically doped, thereby confounding efforts to accurately estimate the effective mobility. The 3 HTMs were significantly dependent on the charge carrier density, indicating that the hole mobility varied among the disordered organic semiconducting materials.[30] The spiro-MeOTAD showed a hole mobility of 10^{-4} to 10^{-3} cm^2 V^{-1} s^{-1}, depending on the photoinduced charge density, which gradually increased in value. The P3HT showed a mobility of around 10^{-3} cm^2 V^{-1} s^{-1}, higher than the value obtained from spiro-MeOTAD but lower than that obtained from PDPPDBTE. A mobility of around 10^{-3} cm^2 V^{-1} s^{-1} was measured for PDPPDBTE, slightly higher than that obtained from P3HT and one order of magnitude higher than that obtained from spiro-MeOTAD at the same charge density. This result indicated that the DPP-based conjugated polymers displayed superior electrical properties. The lower mobility of PDPPDBTE, as measured by TMS, compared to the value obtained from FET measurements

Table 1 Summary of the best-performing device parameters obtained from spiro-MeOTAD, P3HT, and PDPPDBTE

HTM	J_{SC} (mA cm^{-2})	V_{OC} (mV)	FF (%)	PCE (%)
Spiro-MeOTAD	14.3	849.2	62.5	7.6
P3HT	14.0	620.1	72.2	6.3
PDPPDBTE	14.4	855.3	74.9	9.2

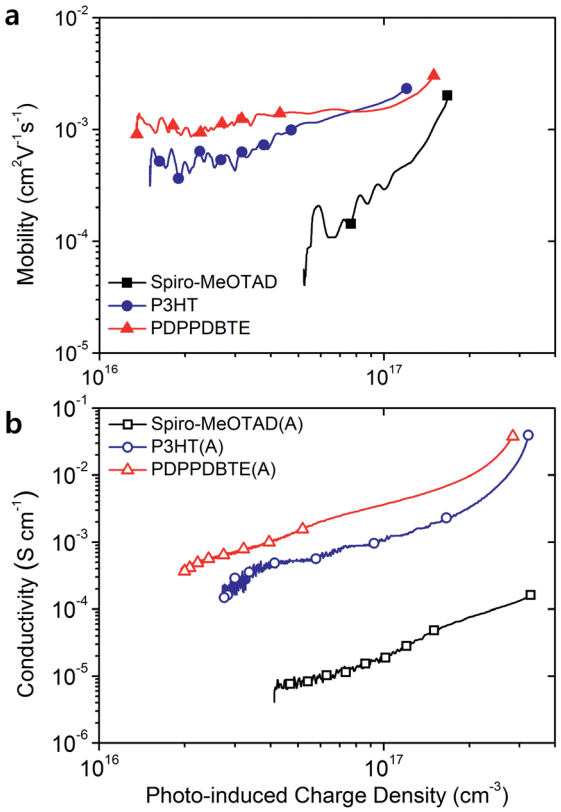

Fig. 3 (a) The effective mobilities of HTMs prepared without additives, as a function of the photoinduced charge density. (b) The effective conductivities of the HTMs. All HTMs were prepared by mixing with Li-TFSI and tBP additives during device fabrication (denoted by HTM(A)).

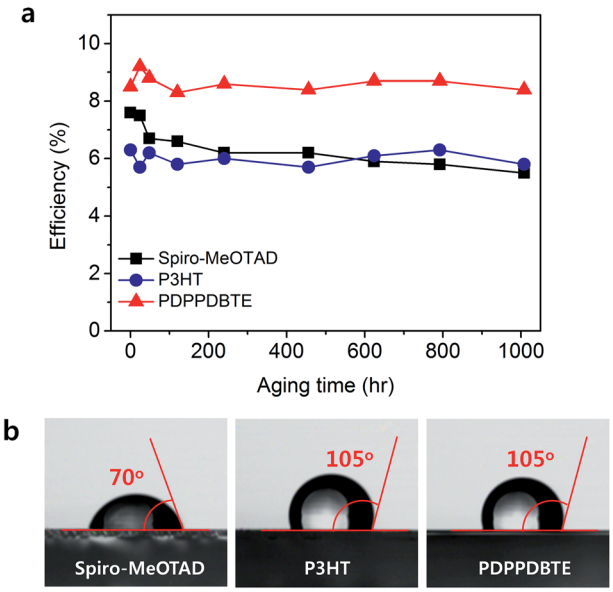

Fig. 4 (a) Long-term stability of spiro-MeOTAD (black), P3HT (red), and PDPPDBTE (blue)-containing hybrid solar cells prepared without encapsulation under a 20% humidity atmosphere. (b) Water contact angles of the spiro-MeOTAD, P3HT, and PDPPDBTE-coated films on an FTO substrate.

($0.32\ cm^2\ V^{-1}\ s^{-1}$)[24] may have been due to (i) the poor crystallinity of the polymer in combination with the mesoporous TiO_2, which provided a mesoscopic architecture (ii) less efficient pore penetration into the mesoporous TiO_2,[31,32] or (iii) higher charge density for measuring FET mobilities.

The conductivity of the 3 HTMs in the presence of Li-TFSI and tBP depended on the charge density, as plotted in Fig. 3b. With the aid of additives, the conductivity of the HTMs could be enhanced because the Li-TFSI tended to form p-doped HTMs.[33,34] The hybrid solar cells were prepared using the HTMs mixed with the additive. The doped spiro-MeOTAD showed a conductivity of 10^{-4} S cm^{-1}, the P3HT yielded a conductivity of 2×10^{-3} S cm^{-1}, and the PDPPDBTE yielded a conductivity of 10^{-2} S cm^{-1} at higher charge densities. The conductivities of the HTMs at a given photo-induced charge density increased from the spiro-MeOTAD to the P3HT and finally to the PDPPDBTE, consistent with the results obtained from the photovoltaic measurements. The fill factors in the devices followed a trend identical to that found among the conductivities and mobilities, ascribed to a reduced series resistance and charge transport in the PDPPDBTE and P3HT.

Finally, the long-term stabilities of the solid-state hybrid solar cells prepared without encapsulation and stored in air at room temperature were tested. Although Kim *et al.* reported that perovskite-based solar cells were stable over 500 hours without encapsulation[4] it has been known that perovskites easily decompose under humid conditions as a result of water adsorption, yielding an ammonium salt.[35] We maintained the humidity of the atmosphere at ~20% and tested the long-term stability of the devices over 1000 hours. Fig. 4a shows that the overall performances of the spiro-MeOTAD cells gradually decreased as the aging time increased, indicating that the moisture may affect the perovskite properties. After 1000 hours of aging, the PCE decreased from 7.6% to 5.5%, a 28% reduction relative to the initial PCE, mainly due to a reduced J_{SC} (Fig. S5†). The stability of the PDPPDBTE cells improved remarkably, and the initial performance was maintained at an 8.4% PCE after 1000 h. The excellent stability of the PDPPDBTE cell may have been due to the hydrophobic properties of the hole transporting layer, which prevented water penetration into the perovskite surface. As shown in Fig. 4b, the water contact angles of the HTM-coated films were 70° for spiro-MeOTAD and 105° for both P3HT and PDPPDBTE. These values were consistent with the excellent stability of the P3HT and PDPPDBTE-based hybrid solar cells. The enhanced stabilities for polymer-based hybrid solar cells were remarkable when considering the much thinner overlayer for polymers, indicating that the hydrophobic nature of HTMs seemed to be strongly related to the stability of the perovskite-based hybrid solar cells.

Conclusions

In summary, we successfully fabricated efficient solid-state organic–inorganic hybrid solar cells based on a $CH_3NH_3PbI_3$ perovskite and a PDPPDBTE hole transport polymer. The solar cell prepared with PDPPDBTE displayed a considerably higher performance than that prepared with the spiro-MeOTAD and

the well-known polymer P3HT. This result was attributed to the enhanced V_{OC} and fill factor. An appropriately deep HOMO energy level conveyed unique charge transport properties onto the PDPPDBTE, which functioned remarkably well as an alternative HTM material and led to a PCE of 9.2%. The long-term stability of the PDPPDBTE devices, as measured over 1000 hours under a humid atmosphere, guarantees the practical applicability of these solid-state hybrid solar cells under outdoor working conditions. These results suggest a broad strategy for developing efficient organic semiconductors, and further enhancements may potentially be realized by carefully tuning the energetic distributions of the HTP and perovskite.

Acknowledgements

This work was supported by the Nano Material Technology Development Program (2012M3A7B4049989), the National Research Foundation of Korea (NRF) grant funded by the Korea government (MSIP) for the Center for Next Generation Dye-Sensitized Solar Cells (no. 2008-0061903). This work was also supported by the Center for Advanced Soft Electronics under the Global Frontier Research Program (Code no. NRF-2012M3A6A5055225) through the NRF funded by the MEST (Korea).

Notes and references

1 U. Bach, D. Lupo, P. Comte, J. E. Moser, F. Weissörtel, J. Salbeck, J. H. Spreitzer and M. Grätzel, *Nature*, 1998, **395**, 583.
2 A. Kojima, K. Teshima, Y. Shirai and T. Miyasaka, *J. Am. Chem. Soc.*, 2009, **131**, 6050.
3 J.-H. Im, C.-R. Lee, J.-W. Lee, S.-W. Park and N.-G. Park, *Nanoscale*, 2011, **3**, 4088.
4 H.-S. Kim, C.-R. Lee, J.-H. Im, K.-B. Lee, T. Moehl, A. Marchioro, A. S.-J. Moon, R. Humphry-Baker, J.-H. Yum, J. E. Moser, M. Grätzel and N.-G. Park, *Sci. Rep.*, 2012, **2**, 591.
5 J. Burschka, N. Pellet, S.-J. Moon, R. Humphry-Baker, P. Gao, M. K. Nazeeruddin and M. Grätzel, *Nature*, 2013, **499**, 316.
6 M. Z. Liu, M. B. Johnston and H. J. Snaith, *Nature*, 2013, **501**, 395.
7 J.-H. Heo, S. H. Im, J. H. Noh, T. N. Mandal, C.-S. Lim, J. A. Chang, Y. H. Lee, H.-J. Kim, A. Sarkar, M. K. Nazeeruddin, M. Grätzel and S. I. Seok, *Nat. Photonics*, 2013, **7**, 486.
8 D. Q. Bi, L. Yang, G. Boschloo, A. Hagfeldt and E. M. J. Johansson, *J. Phys. Chem. Lett.*, 2013, **4**, 1532.
9 B. Cai, Y. D. Xing, Z. Yang, W.-H. Zhang and J. S. Qiu, *Energy Environ. Sci.*, 2013, **6**, 1480.
10 L. Etgar, P. Gao, Z. Xue, Q. Peng, A. K. Chandiran, B. Liu, M. K. Nazeeruddin and M. Grätzel, *J. Am. Chem. Soc.*, 2012, **134**, 17396.
11 D. Poplavskyy and J. Nelson, *J. Appl. Phys.*, 2003, **93**, 341.
12 J. Burschka, A. Dualeh, F. Kessler, E. Baranoff, N. L. Cevey-Ha, C. Y. Yi, M. K. Nazeeruddin and M. Grätzel, *J. Am. Chem. Soc.*, 2011, **133**, 18042.
13 T. Leijtens, J. Lim, J. Teuscher, T. Park and H. J. Snaith, *Adv. Mater.*, 2013, **25**, 3227.
14 H. Sirringhaus, N. Tessler and R. H. Friend, *Science*, 1998, **280**, 1741.
15 Q. Pei, G. Yu, C. Zhang, Y. Yang and A. J. Heeger, *Science*, 1995, **269**, 1086.
16 G. Yu, J. Gao, J. C. Hummelen, F. Wudl and A. J. Heeger, *Science*, 1995, **270**, 1789.
17 G. Horowitz, *Adv. Mater.*, 1998, **10**, 365.
18 S. R. Forrest, *Nature*, 2004, **428**, 911.
19 S. H. Im, C.-S. Lim, J. A. Chang, Y. H. Lee, N. Maiti, H.-J. Kim, M. K. Nazeeruddin, M. Grätzel and S. I. Seok, *Nano Lett.*, 2011, **11**, 4789.
20 J. A. Chang, S. H. Im, Y. H. Lee, H.-J. Kim, C.-S. Lim, J. H. Heo and S. I. Seok, *Nano Lett.*, 2012, **12**, 1863.
21 J. B. Xia, N. Masaki, M. Lira-Cantu, Y. Kim, K. J. Jiang and S. Yanagida, *J. Am. Chem. Soc.*, 2008, **130**, 1258.
22 B. Li, L. D. Wang, B. N. Kang, P. Wang and Y. Qiu, *Sol. Energy Mater. Sol. Cells*, 2006, **90**, 549.
23 I. Kang, T. K. An, J.-A. Hong, H.-J. Yun, R. Kim, D. S. Chung, C. E. Park, Y.-H. Kim and S.-K. Kwon, *Adv. Mater.*, 2013, **25**, 524.
24 H. Bronstein, Z. Y. Chen, R. S. Ashraf, W. M. Zhang, J. P. Du, J. R. Durrant, P. S. Tuladhar, K. Song, S. E. Watkins, Y. Geerts, M. M. Wienk, R. A. J. Janssen, T. Anthopoulos, H. Sirringhaus, M. Heeney and I. McCulloch, *J. Am. Chem. Soc.*, 2011, **133**, 3272.
25 B. Walker, J. H. Liu, C. Kim, G. C. Welch, J. K. Park, J. Lin, P. Zalar, C. M. Proctor, J. H. Seo, G. C. Bazan and T.-Q. Nguyen, *Energy Environ. Sci.*, 2013, **6**, 952.
26 J. M. Ball, M. M. Lee, A. Hey and H. J. Snaith, *Energy Environ. Sci.*, 2013, **6**, 1739.
27 S. A. Haque, E. Palomares, B. M. Cho, A. N. M. Green, N. Hirata, D. R. Klug and J. R. Durrant, *J. Am. Chem. Soc.*, 2005, **127**, 3456.
28 G. Grancini, R. S. S. Kumar, A. Abrusci, H.-L. Yip, C.-Z. Li, A.-K. Y. Jen, G. Lanzani and H. J. Snaith, *Adv. Funct. Mater.*, 2012, **22**, 2160.
29 D. Kuciauskas, J. E. Monat, R. Villahermosa, H. B. Gray, N. S. Lewis and J. K. McCusker, *J. Phys. Chem. B*, 2002, **106**, 9347.
30 H. J. Snaith and M. Grätzel, *Phys. Rev. Lett.*, 2007, **98**, 177402.
31 H. C. Yang, T. J. Shin, L. Yang, K. Cho, C. Y. Ryu and Z. N. Bao, *Adv. Funct. Mater.*, 2005, **15**, 671.
32 H. Sirringhaus, P. J. Brown, R. H. Friend, M. M. Nielsen, K. Bechgaard, B. M. W. Langeveld-Voss, A. J. H. Spiering, R. A. J. Janssen, E. W. Meijer, P. Herwig and D. M. de Leeuw, *Nature*, 1999, **401**, 685.
33 U. B. Cappel, T. Daeneke and U. Bach, *Nano Lett.*, 2012, **12**, 4925.
34 A. Abate, T. Leijtens, S. Pathak, J. Teuscher, R. Avolio, M. E. Errico, J. Kirkpatrik, J. M. Ball, P. Docampo, I. McPherson and H. J. Snaith, *Phys. Chem. Chem. Phys.*, 2013, **15**, 2572.
35 J. H. Noh, S. H. Im, J. H. Heo, T. N. Mandal and S. I. Seok, *Nano Lett.*, 2013, **13**, 1764.
36 S. Qu and H. Tian, *Chem. Commun.*, 2012, **48**, 3039.

